The Canadian Mineralogist
Vol. 50, pp. 843-854 (2012)
DOI: 10.3749/canmin.50.4.843

A STRUCTURAL STUDY OF THE LITHIOPHILITE–SICKLERITE SERIES

FRÉDÉRIC HATERT[§]

Laboratoire de Minéralogie, B18, Université de Liège, B–4000 Liège, Belgium

LUISA OTTOLINI

C.N.R.–Istituto di Geoscienze e Georisorse (IGG), Unità di Pavia,Via A. Ferrata 1, I–27100 Pavia, Italy

JOHAN WOUTERS

Laboratoire de Chimie Biologique Structurale, Département de Chimie,
Facultés Universitaires Notre-Dame-de-la-Paix (FUNDP), Rue de Bruxelles 61, B–5000 Namur, Belgium

FRANÇOIS FONTAN[†]

LMTG–UMR 5563, Observatoire Midi-Pyrénées, 14, avenue Edouard Belin, F–31400 Toulouse, France

ABSTRACT

A sample from the Koktokay No. 3 granitic pegmatite, Altai Mountains, northwestern China, which shows a transition from lithiophilite [$LiMn^{2+}PO_4$] to sicklerite [$Li_{1-x}Mn^{2+}PO_4$], was investigated by single-crystal X-ray diffraction, electron-microprobe analysis, and secondary-ion mass spectrometry (SIMS) techniques. Under the polarizing microscope, the sample shows colorless lithiophilite and deep-orange sicklerite, as well as several intermediate phases. The chemical compositions change from $Li_{0.96}(Mn^{2+}_{0.81}Fe^{2+}_{0.09}Fe^{3+}_{0.08})PO_4$ to $Li_{0.69}(Mn^{2+}_{0.62}Mn^{3+}_{0.19}Fe^{3+}_{0.16})PO_4$, and show a progressive decrease of the lithium content from lithiophilite to sicklerite. Five crystals were extracted from the thin section, and their crystal structures were refined in space group *Pbnm*, with unit-cell parameters from *a* 4.736(1), *b* 10.432(2), *c* 6.088(1) Å (lithiophilite), to *a* 4.765(1), *b* 10.338(1), *c* 6.060(1) Å (sicklerite). The olivine-type structures of these phosphates are identical to that of triphylite, and are characterized by two chains of edge-sharing octahedra parallel to the **c** axis. The first chain consists of *M*1 octahedra containing Li atoms and vacancies, and the second chain consists of *M*2 octahedra occupied by Fe and Mn. The significant Mn^{3+} content in sicklerite necessitates a more careful interpretation of the electron-microprobe data, and demonstrates the different mechanisms of oxidation affecting the lithiophilite–sicklerite and triphylite–ferrisicklerite series, respectively.

Keywords: olivine-type phosphates, lithiophilite, sicklerite, crystal chemistry.

SOMMAIRE

Un échantillon de la pegmatite Koktokay No. 3, Altaï, République populaire de Chine, a été étudié par diffraction des rayons X sur monocristaux, et a fait l'objet d'analyses chimiques à la microsonde électronique et à la sonde ionique (SIMS). Cet échantillon montre une transition progressive entre la lithiophilite incolore [$LiMn^{2+}PO_4$] et la sicklérite orange [$Li_{1-x}Mn^{2+}PO_4$], accompagnée de plusieurs phases intermédiaires. Les analyses chimiques indiquent des compositions comprises entre $Li_{0.96}(Mn^{2+}_{0.81}Fe^{2+}_{0.09}Fe^{3+}_{0.08})PO_4$ et $Li_{0.69}(Mn^{2+}_{0.62}Mn^{3+}_{0.19}Fe^{3+}_{0.16})PO_4$, et montrent une diminution progressive du contenu en lithium, lorsque l'on passe de la lithiophilite à la sicklérite. Cinq monocristaux ont été extraits de la lame mince, et leurs structures cristallines ont été affinées dans le groupe spatial *Pbnm*, avec des paramètres de maille compris entre *a* 4,736(1), *b* 10,432(2), *c* 6,088(1) Å (lithiophilite) et *a* 4,765(1), *b* 10,338(1), *c* 6,060(1) Å (sicklérite). La structure de type olivine de ces phosphates est identique à celle de la triphylite, et est constituée de deux chaînes octaédriques parallèles à l'axe cristallographique **c**. La première chaîne contient les octaèdres *M*1 occupés par le lithium et des lacunes, alors que la seconde chaîne contient les octaèdres *M*2 occupés par le fer et le manganèse. La présence de quantités non négligeables de Mn^{3+} dans la sicklérite démontre la nécessité d'interpréter les analyses chimiques à la microsonde électronique avec précaution, et indique également que les processus d'oxydation affectant les solutions solides lithiophilite–sicklérite et triphylite–ferrisicklérite sont génétiquement distincts.

Mots-clés: phosphates à structure olivine, lithiophilite, sicklerite, cristallochimie.

§ *E-mail address*: fhatert@ulg.ac.be
† Deceased July 26, 2007.

Introduction

Iron–manganese phosphates are common accessory minerals in granitic pegmatites, in metamorphic rocks, and in meteorites. In rare-element pegmatites, primary phosphates of the triphylite–lithiophilite series [$Li(Fe^{2+},Mn^{2+})(PO_4)$ – $Li(Mn^{2+},Fe^{2+})(PO_4)$] form masses that can reach several meters in diameter, enclosed in silicates. During the oxidation processes affecting the pegmatites, these olivine-type phosphates transform to ferrisicklerite – sicklerite [$Li_{1-x}(Fe^{3+},Mn^{2+})(PO_4)$ – $Li_{1-x}(Mn^{2+},Fe^{3+})(PO_4)$] and heterosite – purpurite [$(Fe^{3+},Mn^{3+})(PO_4)$ – $(Mn^{3+},Fe^{3+})(PO_4)$] by the substitution mechanism $Li^+ + Fe^{2+} \rightarrow \square + Fe^{3+}$. This oxidation sequence was first observed by Quensel (1937) and confirmed by Mason (1941).

Olivine-type phosphates crystallize in space group *Pbnm* (triphylite: *a* 4.690, *b* 10.286, *c* 5.987 Å), and their crystal structures have been investigated with synthetic samples (Geller & Durand 1960, Yakubovich *et al.* 1977) and minerals (Finger & Rapp 1969, Eventoff *et al.* 1972, Moore 1972, Alberti 1976, Losey *et al.* 2004, Fehr *et al.* 2007). Since Padhi *et al.* (1997) reported the reversible electrochemical extraction of lithium from $LiFePO_4$, olivine-type phosphates $LiMPO_4$ (*M* = Fe, Mn, Co, Ni) have received major attention as candidates for lithium batteries (*e.g.*, Andersson *et al.* 2000, Okada *et al.* 2001, Ravet *et al.* 2003, Prosini *et al.* 2002, Song *et al.* 2002, Takahashi *et al.* 2002, Yang *et al.* 2003, Bramnik *et al.* 2004, Deniard *et al.* 2004, Fehr *et al.* 2007). Recently, Kang & Ceder (2009) have shown that $LiFePO_4$-based batteries can achieve ultrarapid charging and discharging, in 10–20 s, thus reaching the performance of supercapacitors. These exceptional features place $LiFePO_4$ among the best candidates for producing batteries for many applications, such as electric bicycles, electric boats, electric cars, or for the storage of green energy. In order to elucidate the structural modifications induced by the oxidation processes affecting lithiophilite, we decided to investigate a natural sample from the Altai Mountains, China, in which a progressive transition from lithiophilite to sicklerite is observed.

Sample Description and Geological Setting

The sample investigated herein (#K9–5–6) was collected by Dr. François Fontan in the Koktokay No. 3 granitic pegmatite, Altai Mountains, northwestern China. It consists of a hand specimen of 7 × 6 × 4 cm in size, containing quartz, spodumene, lithiophilite and sicklerite. A section in the sample shows a large (3 × 1 cm) crystal of yellowish lithiophilite surrounded by a brownish rim *ca.* 5 mm thick, consisting of sicklerite. In thin section, the lithiophilite is colorless, and the sicklerite is deep orange. Moreover, several grains located between lithiophilite and sicklerite exhibit intermediate colors, ranging from pale yellow to yellow or orange. The contacts between these grains are generally sharp, and correspond to the cleavage planes or to fractures, thus giving the grains unusual angular shapes (Fig. 1a).

Roughly 100,000 pegmatite dykes occur in the Chinese Altai pegmatite field; the Koktokay No. 3 pegmatite is one of the most strongly zoned. This pegmatite, which shows a NW–SE elongation, intrudes a metagabbro located in gneissic biotite schists (Zhang *et al.* 2004), and was formed during the Yanshanian period (177.9–148.0 million years; Chen *et al.* 2000). On the basis of their mineral contents, nine zones were described in the pegmatite, and the sample investigated in this study was collected in zone V, characterized by the presence of bladed albite and spodumene (Zhu *et al.* 2000). Lithiophilite and sicklerite from this zone

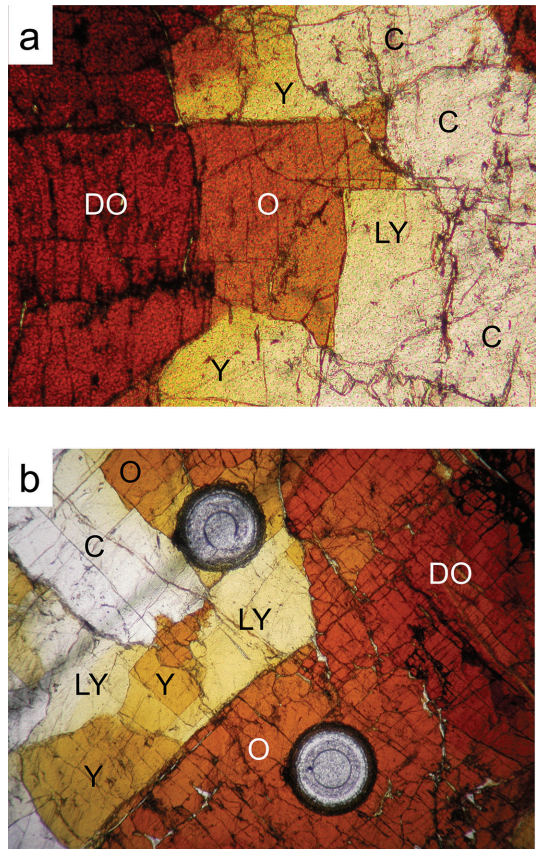

FIG. 1. a. Micrograph showing the transition from lithiophilite (colorless) to sicklerite (deep orange), with several grains exhibiting intermediate colors. b. Thin section after drilling in the orange and yellow zones. Notation: C: colorless lithiophilite, LY: light yellow phase, Y: yellow phase, O: orange phase, DO: deep orange sicklerite. Plane-polarized light; the widths of the photographs are 800 and 1600 μm, respectively.

were previously described by Wang *et al*. (1981), who investigated the X-ray powder diffraction, optical and thermal properties of the phosphates.

Experimental

An electron-microprobe analysis (Table 1) was done with a Cameca SX–50 instrument (Ruhr-Universität Bochum, Germany) operating in the wavelength-dispersion mode with an accelerating voltage of 15 kV and a beam current of 15 nA. The following standards were used: graftonite (P, Mn, Fe), pyrope (Mg), ZnO (Zn), and andradite (Ca). The counting time was 20 s for all elements.

The Li_2O contents (Table 1) were determined with a Cameca IMS–4f ion microprobe (SIMS) installed at CNR–IGG, Pavia, Italy. We used a 12.5 kV accelerated $^{16}O^-$ primary-ion beam with a current intensity in the range 0.8–4 nA, corresponding to a beam diameter of ~3–6 mm. The samples were polished, washed in an ultrasonic tank with ethanol, and Pt-coated (400 Å thickness) before analysis. Secondary-ion signals of the isotopes $^6Li^+$, $^{31}P^+$ and $^{57}Fe^+$ were detected at the electron multiplier. Acquisition times were 3 s for Li and P (each), and 6 s for Fe over three cycles. Analysis was done under steady-state sputtering conditions after sputtering for 360 s using ~75–125 eV secondary ions. The choice of medium- to high-energy secondary ions (energy filtering) as analytical ones is particularly useful to reduce matrix effects affecting light-element ionization and to improve the reproducibility of analysis (Ottolini *et al*. 1993). In the present case, the precision of analyses, as tested on various (CNR–IGG) Li-bearing homogeneous glassy standards, was found to be better or on the order of 1% rel. (as 1σ) over a one-day analytical span. In order to convert the ($^6Li^+/^{31}P^+$ and $^6Li^+/^{57}Fe^+$) ion signals into (Li) concentrations, we used as reference material for SIMS analysis of our material for triphylite from the Buranga pegmatite, Rwanda; more details concerning the SIMS analytical procedure are given by Hatert *et al*. (2011a).

The X-ray study of the structures was done on an Oxford Diffraction Gemini PX Ultra four-circle diffractometer equipped with a Ruby CCD area-detector (Namur, Belgium), on crystal fragments drilled out of the thin section (Fig. 1b). The following numbers were used for the crystals: crystal 1: colorless lithiophilite, crystal 2: light yellow phase, crystal 3: yellow phase, crystal 4: orange phase, and crystal 5: deep orange sicklerite. Between 191 (crystal 1) and 1276 (crystal 3) frames with a spatial resolution of 1° were collected by the ϕ-ω scan technique, with a counting time of 5 to 20 s per frame, in the range $7.82° < 2\theta < 85.50°$. The number of reflections extracted from these frames, as well as the unit-cell parameters of the phosphates, are given in Table 2. Data were corrected for Lorenz, polarization and absorption effects, the latter with an empirical method using the SCALE3 ABSPACK scaling algorithm included in the CrysAlisRED package (Oxford Diffraction 2007).

The structures were refined with SHELXTL (Sheldrick 2008) in space group *Pbnm*, starting from the atom coordinates of lithiophilite used by Losey *et al*. (2004), and scattering curves for neutral atoms, together with anomalous dispersion corrections, taken from the *International Tables for X-ray Crystallography, Vol. C* (Wilson 1992). For the sake of simplicity, Mg, Zn and Ca, which occur in low to trace amounts, were not taken into account in crystal-structure refinement. The relative occupancies of Li and vacancies at *M*1, and of Fe and Mn at *M*2, were refined, with the Mn content of the *M*2 site constrained to 0.800, according to the electron-microprobe analyses (see below). The refinements were completed using anisotropic-displacement parameters for all atoms. The final conventional R_1 factors [$F_0 > 2\sigma(F_0)$] are between 0.0218 and 0.0292; further details of intensity data collection and structure refinement are given in Table 2. A listing of structure factors and a cif file for each refined structure are available from the Depository of Unpublished Data in the Mineralogical Association of Canada website [document Lithiophilite–Sicklerite CM50_843].

TABLE 1. COMPOSITION OF PHOSPHATES OF THE LITHIOPHILITE–SICKLERITE SERIES

Sample	1	2	3	4	5
n	4	6	4	8	6
P_2O_5 wt.%	46.93	46.58	46.82	47.06	47.08
Fe_2O_3*	6.69	3.97	8.44	8.54	8.60
Mn_2O_3*	-	-	0.34	3.12	9.86
MgO	0.10	0.11	0.07	0.08	0.09
ZnO	0.07	0.07	0.07	0.04	0.05
FeO*	1.72	4.34	-	-	-
MnO*	37.59	37.46	37.72	35.47	29.33
CaO	0.05	0.10	0.03	0.05	0.03
Li_2O**	9.21	9.44	8.66	8.11	6.85
Total	102.36	102.07	102.15	102.47	101.89
P *apfu*	1.000	1.000	1.000	1.000	1.000
Fe^{3+}	0.127	0.076	0.160	0.161	0.162
Mn^{3+}	-	-	0.006	0.060	0.188
Mg	0.004	0.004	0.003	0.003	0.003
Zn	0.001	0.001	0.001	0.001	0.001
Fe^{2+}	0.036	0.092	-	-	-
Mn^{2+}	0.801	0.805	0.806	0.754	0.623
Ca	0.001	0.003	0.001	0.001	0.001
Li	0.932	0.963	0.879	0.819	0.691
Fe/(Fe + Mn)	0.169	0.173	0.165	0.165	0.167

Analyst: H.-J. Bernhardt, of Bochum, Germany, carried out the electron-microprobe analyses. Cation numbers were calculated on the basis of one P atom per formula unit. * The FeO/Fe_2O_3 and MnO/Mn_2O_3 values were calculated to maintain charge balance. ** The Li_2O content was determined by SIMS (analyst: Luisa Ottolini). *n*: number of analyses made.

TABLE 2. EXPERIMENTAL DETAILS FOR THE SINGLE-CRYSTAL X-RAY-DIFFRACTION STUDY OF THE LITHIOPHILITE–SICKLERITE SERIES

Sample	1	2	3	4	5
Color	Colorless	Light yellow	Yellow	Orange	Deep orange
Dimensions of the crystal (mm)	*ca.* 0.08 × 0.08 × 0.03	*ca.* 0.08 × 0.08 × 0.03	*ca.* 0.08 × 0.08 × 0.03	*ca.* 0.08 × 0.08 × 0.03	*ca.* 0.08 × 0.08 × 0.03
a (Å)	4.736(1)	4.734(1)	4.740(1)	4.767(1)	4.765(1)
b (Å)	10.432(2)	10.423(2)	10.415(1)	10.403(2)	10.338(1)
c (Å)	6.088(1)	6.094(1)	6.080(1)	6.072(1)	6.060(1)
Space group	*Pbnm*	*Pbnm*	*Pbnm*	*Pbnm*	*Pbnm*
Z	4	4	4	4	4
$2\theta_{min}$, $2\theta_{max}$	7.82°, 65.20°	7.82°, 65.16°	7.82°, 85.50°	7.84°, 64.88°	7.88°, 85.50°
Range of indices	$-7 \le h \le 3$, $-8 \le k \le 15$, $-9 \le l \le 7$	$-7 \le h \le 6$, $-7 \le k \le 15$, $-8 \le l \le 7$	$-8 \le h \le 7$, $-18 \le k \le 18$, $-10 \le l \le 10$	$-6 \le h \le 7$, $-8 \le k \le 15$, $-6 \le l \le 9$	$-8 \le h \le 7$, $-19 \le k \le 18$, $-10 \le l \le 10$
Measured intensities	1539	1653	5279	1515	5167
Unique reflections	545	548	1095	547	1066
Independent non-zero [$I > 2\sigma(I)$] reflections	480	492	891	464	876
μ (mm^{-1})	4.862	4.895	4.872	4.888	4.899
Refined parameters	42	42	42	42	42
R_1 [$F_o > 2\sigma(F_o)$]	0.0235	0.0219	0.0292	0.0250	0.0218
R_1 (all)	0.0278	0.0260	0.0376	0.0320	0.0298
wR_2 (all)	0.0622	0.0580	0.0635	0.0605	0.0541
S (goodness of fit)	1.003	0.949	1.062	0.992	1.052
Max. Δ/σ in the last least-squares cycle	0.000	0.000	0.000	0.000	0.000
Max. peak and hole in the final Δ*F* map (*e*/Å^3)	+0.64 and –0.60	+0.66 and –0.51	+1.89 and –0.81	+0.83 and –0.51	+1.19 and –0.56

Chemical Variations along the Lithiophilite–Sicklerite Series

Under the polarizing microscope, lithiophilite is colorless, whereas sicklerite is deep orange. Several grains also show intermediate colors (Fig. 1), suggesting a progressive transition from lithiophilite to sicklerite. The SIMS results for Li_2O (wt.%) are: Sample 1 (four analyses): 9.21 ± 0.11 (1.2 as 1σ); sample 2 (four analyses): 9.44 ± 0.04 (0.5 as 1σ); sample 3 (six analyses): 8.66 ± 0.56 (6.5 as 1σ); sample 4 (six analyses): 8.11 ± 0.30 (3.7 as 1σ); sample 5 (six analyses): 6.85 ± 0.35 (5.0 as 1σ). These data indicate a higher micro-scale inhomogeneity of Li in samples 3, 4, and 5. Nevertheless, the progressive transition observed optically is confirmed by results of the SIMS analyses, which indicate Li values from 0.963 (lithiophilite) to 0.691 (sicklerite) Li atoms per formula unit (*apfu*) (Table 1). The charge deficit induced by this leaching of Li is compensated by progressive oxidation of Fe^{2+} to Fe^{3+} (samples 1 to 3), followed by oxidation of Mn^{2+} to Mn^{3+} (samples 3 to 5; Table 1). Moreover, it seems that the presence of Mn^{3+} in sicklerite is correlated with the strong orange color of the samples, clearly visible in crystals 3, 4, and 5 (Fig. 1).

It is noteworthy that this progressive oxidation does not induce significant variations of Fe/(Fe + Mn), which ranges between 0.165 and 0.173 (Table 1). This constancy of the Fe/(Fe + Mn) value is well established during the oxidation of triphylite (*e.g.,* Fransolet *et al.* 1985, 1986, Roda *et al.* 1996, 2004, Roda-Robles *et al.* 1998, 2010), and is due to the topotactic nature of this oxidation process, which preserves the olivine structure-type of the parent phosphates.

Structure Refinement

Final positional and equivalent isotropic-displacement parameters are given in Table 3, and selected interatomic distances and angles are given in Table 4. The structure is identical to that of triphylite (Losey *et al.* 2004), and is characterized by two chains of edge-sharing octahedra parallel to the **c** axis: a first chain consists of *M*1 octahedra containing Li atoms and vacancies, and the second chain is formed by the *M*2 sites, occupied by Fe and Mn. The chains are connected in the **b** direction by a sharing of edges of the octahedra, and the resulting sheets are connected in the **a** direction by PO_4 tetrahedra (Fig. 2).

A detailed distribution of cations has also been established by taking into account the results of the chemical analyses and of the single-crystal structure refinement. The results given in Table 5 indicate that the refined site-populations (RSP) obtained from the single-crystal structure refinement are in good agreement with the assigned site-populations (ASP) deduced from the electron-microprobe and SIMS results. Moreover, the refined site-scattering values (RSS) and the mean bond-

lengths (MBL) obtained from the structure refinement are very close to the calculated site- scattering values (CSS) and the calculated bond-lengths (CBL), respectively (Table 5). This agreement again confirms the reliability of the site populations assigned.

Finally, the bond-valence sums were calculated as $s = \exp[(R_0 - R)/0.37]$, by using the R_0 values of Brown & Altermatt (1985). The sums for O and P atoms are in the ranges 1.84–2.02 and 4.90–4.93 *vu*, respectively, in good agreement with their ideal values. For the *M*2 site, the bond-valence sums show a significant increase from 2.01 (crystal 1) to 2.12 *vu* (crystal 5) (Fig. 3b), due to the progressive oxidation of Fe and Mn at that site, which produces a decrease of the mean *M*2–O bond lengths (Table 4). Conversely, a decrease in the sums is observed at the *M*1 site, from 0.93 (crystal 1) to 0.87 *vu* (crystal 5) (Fig. 3a), correlated with an increase of the *M*1–O bond lengths (Table 4). This decrease of the bond-valence sum at the *M*1 site is due to decrease of the Li occupancy at that site (Table 3).

TABLE 3. FINAL FRACTIONAL COORDINATES AND EQUIVALENT DISPLACEMENT PARAMETERS (Å²) OF ATOMS IN PHOSPHATES OF THE LITHIOPHILITE–SICKLERITE SERIES

Site	Atom	*x*	*y*	*z*	U_{eq}
		Sample 1: Colorless			
*M*1	Li*	0	0	0	0.016(2)
*M*2	Mn, Fe*	0.97196(9)	0.28174(4)	¼	0.0072(1)
P	P	0.4104(1)	0.09276(7)	¼	0.0065(2)
O1	O	0.7321(4)	0.0969(2)	¼	0.0099(4)
O2	O	0.2111(4)	0.4560(2)	¼	0.0088(4)
O3	O	0.2776(3)	0.1621(1)	0.0490(2)	0.0095(3)
		Sample 2: Light yellow			
*M*1	Li*	0	0	0	0.014(2)
*M*2	Mn, Fe*	0.97198(8)	0.28175(3)	¼	0.0081(1)
P	P	0.4103(1)	0.09283(6)	¼	0.0076(2)
O1	O	0.7318(4)	0.0971(2)	¼	0.0114(4)
O2	O	0.2106(3)	0.4559(2)	¼	0.0101(3)
O3	O	0.2784(2)	0.1621(1)	0.0490(2)	0.0103(3)
		Sample 3: Yellow			
*M*1	Li*	0	0	0	0.017(1)
*M*2	Mn, Fe*	0.97167(6)	0.28160(2)	¼	0.00845(7)
P	P	0.41062(8)	0.09310(4)	¼	0.0071(1)
O1	O	0.7308(2)	0.0981(1)	¼	0.0115(2)
O2	O	0.2081(2)	0.4557(1)	¼	0.0103(2)
O3	O	0.2772(2)	0.16258(7)	0.0490(1)	0.0109(2)
		Sample 4: Orange			
*M*1	Li*	0	0	0	0.019(2)
*M*2	Mn, Fe*	0.97049(9)	0.28133(4)	¼	0.0079(1)
P	P	0.4108(1)	0.09375(7)	¼	0.0079(2)
O1	O	0.7299(5)	0.1007(2)	¼	0.0137(4)
O2	O	0.2030(4)	0.4555(2)	¼	0.0126(4)
O3	O	0.2763(3)	0.1637(2)	0.0497(2)	0.0131(3)
		Sample 5: Deep orange			
*M*1	Li*	0	0	0	0.022(2)
*M*2	Mn, Fe*	0.97002(5)	0.28118(2)	¼	0.00931(6)
P	P	0.41101(8)	0.09406(3)	¼	0.00849(9)
O1	O	0.7292(3)	0.1021(1)	¼	0.0150(2)
O2	O	0.2001(3)	0.45515(9)	¼	0.0136(2)
O3	O	0.2759(2)	0.16404(7)	0.0492(1)	0.0142(2)

* The occupancy factors for the *M*1 and *M*2 sites are as follows. Sample 1: 0.91(3) Li and 0.800 Mn + 0.183(3) Fe; sample 2: 0.86(3) Li and 0.800 Mn + 0.183(3) Fe; sample 3: 0.84(2) Li and 0.800 Mn + 0.200(2) Fe; sample 4: 0.76(3) Li and 0.800 Mn + 0.180(3) Fe; sample 5: 0.75(2) Li and 0.800 Mn + 0.195(2) Fe.

Discussion

Crystal chemistry of the lithiophilite–sicklerite series

Variations in the unit-cell parameters along the triphylite–lithiophilite series were investigated by X-ray powder diffraction (Fransolet *et al.* 1984) and single-crystal X-ray diffraction (Losey *et al.* 2004); these studies show a significant increase of the unit-cell parameters as Fe/(Fe + Mn) decreases. In the lithiophilite–sicklerite series, a different pattern of behavior is observed, with a decrease in *b* and *c*, but an increase in *a*, as the lithium content decreases (Fig. 4). The increase in *a* can be explained by the increase of the *M*1–O1 and *M*1–O2 bond lengths, which form a square parallel to the **a** axis (Table 4, Fig. 5a), whereas the decrease of *b* is correlated with a decrease of the *M*2–O1 and *M*2–O2 bond lengths, which are parallel to the **b** axis (Table 4, Fig. 5b).

In the triphylite–lithiophilite series, Losey *et al.* (2004) observed a decrease of the *M*2–O bond lengths as Mn^{2+} (effective ionic radius, *e.i.r.*, 0.830 Å; Shannon 1976) is replaced by Fe^{2+} (*e.i.r.* 0.780 Å; Shannon 1976). This decrease is positively correlated with a decrease of the *M*1–O bond lengths, except for the *M*1–O3 bonds, which increase significantly. As Fe and Mn occur at the *M*2 site in olivine-type phosphates, the decrease of *M*2–O bond lengths was expected by Losey *et al.* (2004), but the decrease of *M*1–O bond lengths is more difficult to understand because this site is solely occupied by Li in this series. In the lithiophilite–sicklerite series, a global decrease of the *M*2–O bond lengths is observed, produced by oxidation of Fe^{2+} and Mn^{2+} to Fe^{3+} (*e.i.r.* 0.645 Å; Shannon 1976) and Mn^{3+} (*e.i.r.* 0.645 Å; Shannon 1976), respectively (Fig. 6b). Simultaneous with this oxidation, the lithium content decreases at *M*1, inducing an increase of the *M*1–O distances necessary to satisfy bond-valence requirements (Fig. 6a). As a consequence, the *M*1–O and *M*2–O bond distances negatively correlate with each other in the lithiophilite–sicklerite series, whereas they are positively correlated to each other in the triphylite–lithiophilite series. The negative correlation observed in the lithiophilite–sicklerite series is governed mainly by charge-balance requirements, which necessitate a decrease in the Li content at *M*1 in order to compensate the oxidation of Fe and Mn at *M*2. This correlation is also certainly influenced by crystal-chemical constraints: indeed, the olivine structure is extremely compact, and each oxygen atom is bonded to both *M*1 and *M*2 cations, thus explaining why a volume increase

TABLE 4. SELECTED BOND-DISTANCES (Å) AND ANGLES (°) FOR PHOSPHATES OF THE LITHIOPHILITE–SICKLERITE SERIES

Sample	1	2	3	4	5	Difference
*M*1-O1 × 2	2.224(1)	2.227(1)	2.2319(9)	2.249(2)	2.2527(9)	+0.029
*M*1-O2 × 2	2.098(1)	2.100(1)	2.1065(8)	2.127(2)	2.1334(9)	+0.035
*M*1-O3 × 2	2.163(1)	2.164(1)	2.1639(9)	2.174(2)	2.1663(8)	+0.003
Mean	2.162	2.164	2.167	2.183	2.184	+0.022
*M*2-O1	2.238(2)	2.235(2)	2.226(1)	2.201(2)	2.178(1)	-0.060
*M*2-O2	2.142(2)	2.138(2)	2.132(1)	2.124(2)	2.106(1)	-0.036
*M*2-O3 × 2	2.122(1)	2.122(1)	2.1194(8)	2.120(1)	2.1127(8)	-0.009
*M*2-O3' × 2	2.270(1)	2.271(1)	2.2644(9)	2.259(2)	2.2519(8)	-0.018
Mean	2.194	2.193	2.188	2.181	2.169	-0.025
P-O1	1.524(2)	1.523(2)	1.519(1)	1.523(2)	1.518(1)	-0.006
P-O2	1.538(2)	1.538(2)	1.537(1)	1.537(2)	1.531(1)	-0.007
P-O3 × 2	1.554(1)	1.553(1)	1.5546(8)	1.555(2)	1.5551(7)	+0.001
Mean	1.543	1.542	1.541	1.543	1.540	-0.003
O1-P-O2	113.5(1)	113.5(1)	113.43(6)	113.4(1)	113.39(6)	
O1-P-O3 × 2	113.04(7)	112.85(6)	112.99(4)	112.92(7)	112.82(4)	
O2-P-O3 × 2	106.28(7)	106.37(6)	106.52(4)	106.99(8)	107.05(4)	
O3-P-O3	103.9(1)	104.1(1)	103.63(7)	102.9(1)	102.96(6)	
Mean	109.34	109.34	109.35	109.35	109.35	

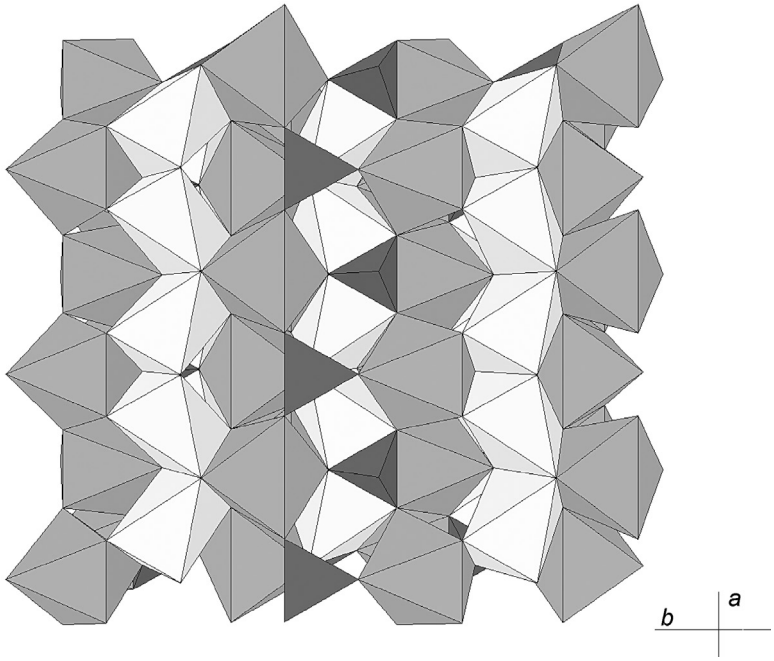

FIG. 2. The crystal structure of sicklerite, projected perpendicular to the **c** axis. The *M*1 octahedra containing Li are white, the *M*2 octahedra containing Fe and Mn are light grey, and the PO_4 tetrahedra are dark grey.

of one of these sites implies a volume decrease of the adjacent polyhedron.

Finally, bond-length distortion (BLD) for the *M*1 and *M*2 sites was calculated with the formula of Renner & Lehmann (1986). As shown on Figure 7, the BLD coefficient for *M*1 decreases linearly with increasing Li content (Fig. 7a), whereas the BLD coefficient on *M*2 shows the inverse behavior (Fig. 7b). The low BLD coefficient for the *M*2 site of sicklerite is unexpected, as Eventoff *et al*. (1972) noticed that the complete oxidation of iron and manganese induces a Jahn–Teller distortion of the $M(2)O_6$ octahedron in heterosite, characterized by two short bonds (1.912–1.914 Å) and four long bonds (2.030–2.163 Å). Such a strong distortion of the *M*2 octahedron is not observed in sicklerite, but the presence of larger amounts of Mn^{3+} at that site in purpurite would certainly increase significantly the BLD, as shown by Hatert *et al*. (2011b) in the series triphylite – ferrisicklerite – heterosite. Conversely, the increase of the BLD coefficient of *M*1, observed as the Li content decreases (Fig. 7a), is certainly due to the partial occupancy of that site. Indeed, the average ionic radius at *M*1 decreases significantly as the Li content decreases, owing to the presence of vacancies, and the coordination polyhedron consequently becomes too large. According to the distortion theorem (Brown 2002), any anion located in too large a cavity will induce a distortion of its environment in order to increase the bond-valence sum to the expected value, thus explaining the increase of *M*1 BDL in Li-poor members of the lithiophilite–sicklerite series (Fig. 7a).

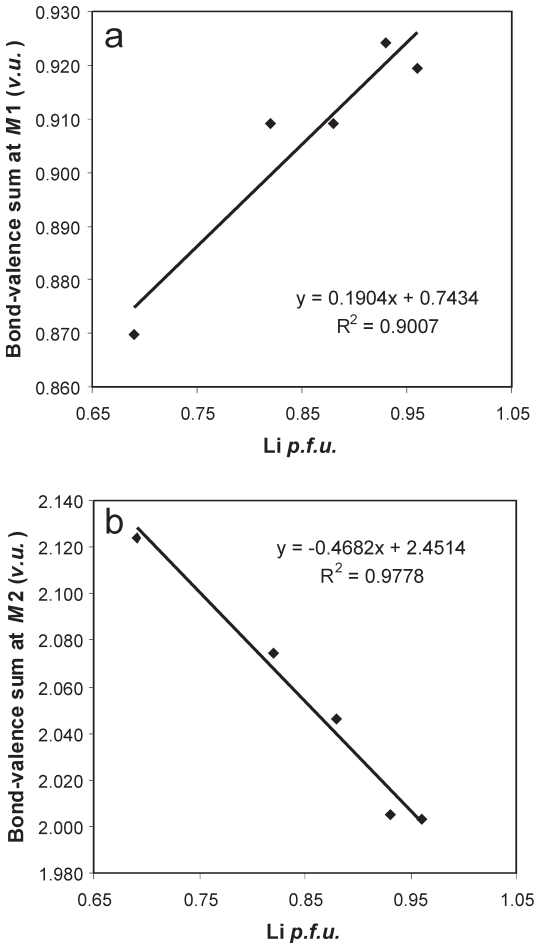

FIG. 3. Variations of bond-valence sums at the *M*1 (a) and *M*2 (b) crystallographic sites, along the lithiophilite–sicklerite series.

Chemistry, nomenclature, and stability of sicklerite

The lithium contents determined by SIMS in members of the lithiophilite–sicklerite series (Table 1) are in good agreement with the Li values determined by refinement of the *M*1 site-occupancy factors (Table 3), thus confirming the reliability of the SIMS analytical procedure applied here. A comparison of the Li content of sicklerite from the Altai Mountains with those of sicklerite from Pala, San Diego County, California (Schaller 1912), Wodgina, Western Australia, and Eräjärvi, Finland (Mason 1941), shows a higher Li content for the sample investigated here (Table 1). As a consequence, we take note of the unexpected variability of the Li content in sicklerite, which ranges from 6.85 to 3.80 wt.% Li_2O. Moreover, the existence of intermediate phases, characterized by Li contents between 9.44 and 8.11 wt.% Li_2O, raises an important nomenclature question: where is the boundary between sicklerite and lithiophilite? According to Fontan *et al*. (1976), the distinction between these species is based mainly on their optical properties and their color; consequently, crystals 1 and 2, showing light colors (Fig. 1), can be considered as lithiophilite, whereas crystals 3, 4, and 5, with strong colors and containing significant amounts of Mn^{3+} (Fig. 1, Table 1), correspond to sicklerite. As these minerals were historically defined on the basis of their optical properties, it is difficult to apply the dominant-constituent rule in this case (Hatert & Burke 2008). However, new analyses on these phosphates are being conducted in order to elucidate this delicate question in nomenclature issues.

The interpretation of the electron-microprobe analyses of sicklerite is based on the assumption that the mineral contains Fe^{3+} and Mn^{2+}, but no Mn^{3+}. This hypothesis, from which Li contents of sicklerite samples are estimated, is clearly ruled out by the chemical data presented here, which show up to 9.86 wt.% Mn_2O_3 in crystal 5 (Table 1). Moreover, the presence of significant amounts of Mn^{3+} in sicklerite was already mentioned by Fontan *et al*. (1976), and the wet-chemical analyses reported by Palache *et al*. (1951) show Mn^{3+} contents

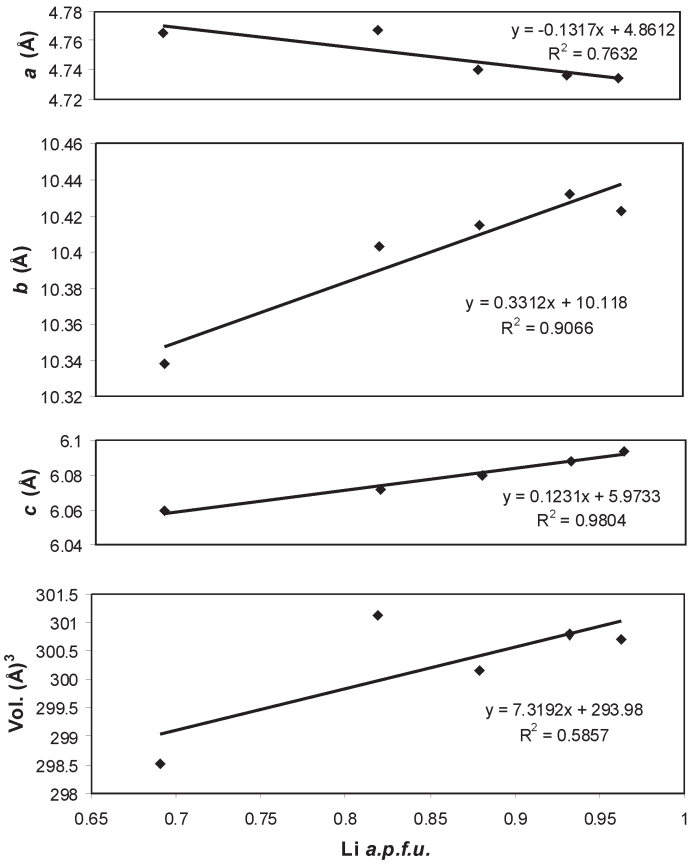

FIG. 4. Variations of the unit-cell parameters along the lithiophilite–sicklerite series.

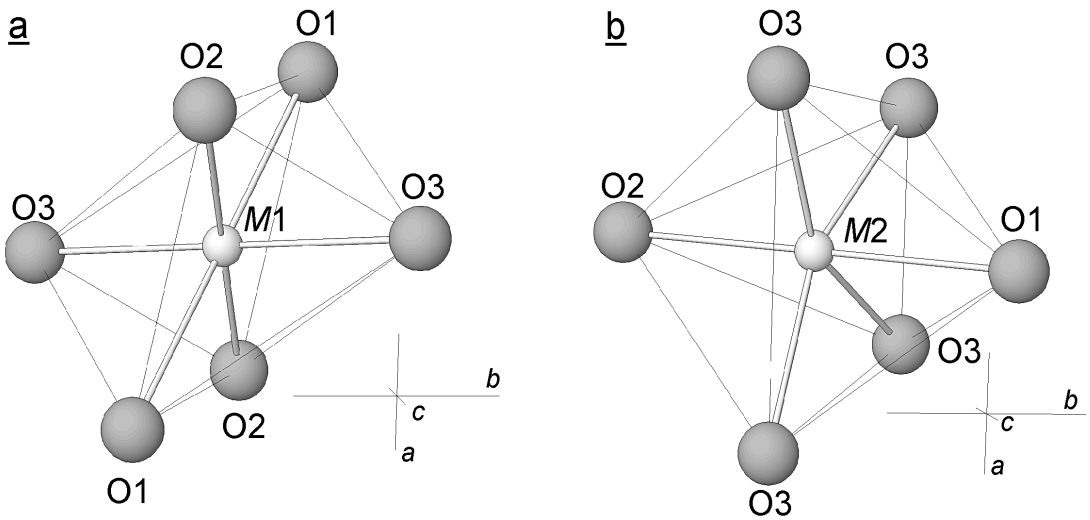

FIG. 5. Morphologies of the *M*1 (a) and *M*2 (b) octahedrally coordinated sites in the crystal structure of sicklerite.

TABLE 5. REFINED SITE-POPULATIONS (RSP, *apfu*), REFINED SITE-SCATTERING VALUES (RSS, *epfu*), MEAN BOND-LENGTHS (MBL, Å), ASSIGNED SITE-POPULATIONS (ASP, *apfu*), CALCULATED SITE-SCATTERING VALUES (CSS, *epfu*), AND CALCULATED BOND-LENGTHS (CBL, Å) IN PHOSPHATES OF THE LITHIOPHILITE–SICKLERITE SERIES

	Results of the structure determination			Results of the chemical analysis		
Site	RSP	RSS	MBL	ASP	CSS	CBL*
	Sample 1: Colorless					
*M*1	0.91(3) Li	2.7	2.162	0.932 Li	2.8	2.160
*M*2	0.800 Mn + 0.183(3) Fe	24.8	2.194	0.800 Mn^{2+} + 0.150 Fe^{3+} + 0.050 Fe^{2+}	25.2	2.200
	Sample 2: Light yellow					
*M*1	0.86(3) Li	2.6	2.164	0.963 Li	2.9	2.160
*M*2	0.800 Mn + 0.183(3) Fe	24.8	2.193	0.800 Mn^{2+} + 0.100 Fe^{3+} + 0.100 Fe^{2+}	25.2	2.207
	Sample 3: Yellow					
*M*1	0.84(2) Li	2.5	2.168	0.879 Li	2.6	2.160
*M*2	0.800 Mn + 0.200(2) Fe	25.2	2.188	0.800 Mn^{2+} + 0.150 Fe^{3+} + 0.050 Mn^{3+}	25.2	2.193
	Sample 4: Orange					
*M*1	0.76(3) Li	2.3	2.183	0.819 Li	2.5	2.160
*M*2	0.800 Mn + 0.180(3) Fe	24.7	2.181	0.750 Mn^{2+} + 0.150 Fe^{3+} + 0.100 Mn^{3+}	25.2	2.184
	Sample 5: Deep orange					
*M*1	0.75(2) Li	2.2	2.184	0.691 Li	2.1	2.160
*M*2	0.800 Mn + 0.195(2) Fe	25.1	2.169	0.650 Mn^{2+} + 0.150 Fe^{3+} + 0.200 Mn^{3+}	25.2	2.165

* The CBL values have been calculated from the ASP with the effective ionic radii of Shannon (1976), assuming a full occupancy of the crystallographic sites.

between 2.10 and 8.19 wt.% Mn_2O_3. Consequently, the Li contents of sicklerite samples estimated from electron-microprobe data are not reliable.

As underlined by Fontan *et al*. (1976), the presence of significant amounts of Mn^{3+} in sicklerite, and its near-absence from ferrisicklerite, indicate different processes of formation for these two phosphates. This distinction is confirmed by the petrographic and chemical observations given in the present paper, which clearly show a progressive transition from lithiophilite to sicklerite (Fig. 1, Table 1), never observed in the triphylite–ferrisicklerite series. These different processes of oxidation, certainly controlled by the distinct geochemical behaviors of iron and manganese, are also responsible for the thermal instability of synthetic purpurite, which transforms to $Mn_2P_2O_7$ above 210°C, whereas synthetic heterosite, its Fe^{3+}-dominant analogue, is stable up to a high temperature (Kim *et al*. 2009, Chen & Richardson 2010).

ACKNOWLEDGEMENTS

This paper is dedicated to Petr Černý, in recognition of his incommensurate contributions to pegmatology. The authors acknowledge reviewers F.C. Hawthorne and J.M. Hughes for their helpful comments, R.F. Martin and M. Galliski for the editorial handling of the manuscript, Ru-Cheng Wang for his help during the field trip in China, H.-J. Bernhardt for the electron-microprobe analyses, as well as financial support of the FRS–F.N.R.S. (Belgium) for a position of "Chercheur Qualifié" (F.H.).

REFERENCES

ALBERTI, A. (1976): The crystal structure of ferrisicklerite, $Li_{<1}(Fe^{3+},Mn^{2+})PO_4$. *Acta Crystallogr*. **B32**, 2761-2764.

ANDERSSON, A.S., KALSKA, B., HÄGGSTRÖM, L. & THOMAS, J.O. (2000): Lithium extraction/insertion in $LiFePO_4$: an X-ray diffraction and Mössbauer spectroscopy study. *Solid State Ionics* **130**, 41-52.

BRAMNIK, N.N., BRAMNIK, K.G., BUHRMESTER, T., BAEHTZ, C., EHRENBERG, E. & FUESS, H. (2004): Electrochemical and structural study of $LiCoPO_4$-based electrodes. *J Solid State Electrochem*. **8**, 558-564.

BROWN, I.D. (2002): *The Chemical Bond in Inorganic Chemistry*. Oxford University Press, New York, N.Y.

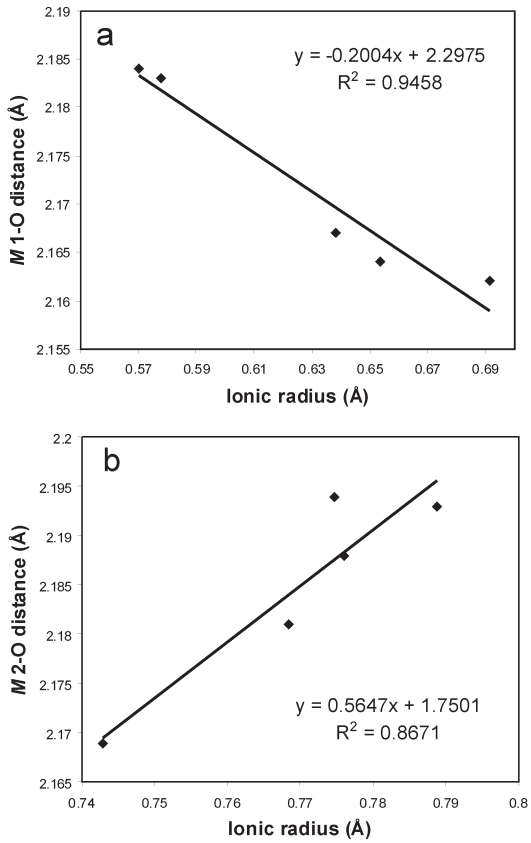

FIG. 6. Correlations between the *M*–O distances and the mean ionic radii of the cations occurring at the *M*1 (a) and *M*2 (b) sites in the lithiophilite–sicklerite series.

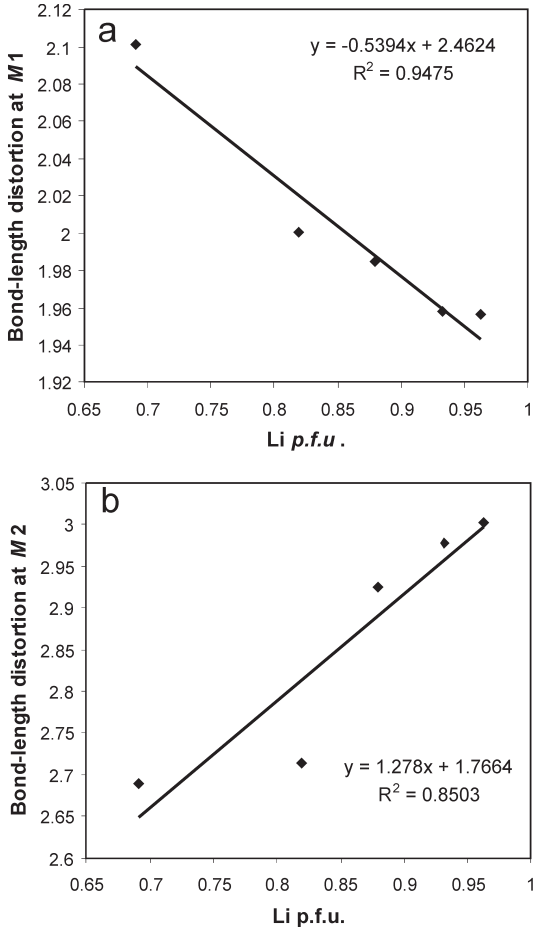

FIG. 7. Variations of bond-length distortion at *M*1 (a) and *M*2 (b) along the lithiophilite–sicklerite series.

BROWN, I.D. & ALTERMATT, D. (1985): Bond-valence parameters obtained from a systematic analysis of the inorganic crystal structure database. *Acta Crystallogr.* **B41**, 244-247.

CHEN, F.W., LI, H.Q., WANG, D.H., CAI, H. & CHEN, W. (2000): New chronological evidence for Yanshanian diagenetic mineralization in China's Altay orogenic belt. *Chinese Science Bull.* **45**, 108-114.

CHEN, G. & RICHARDSON, T.J. (2010): Thermal instability of olivine-type $LiMnPO_4$ cathodes. *J. Power Sources* **195**, 1221-1224.

DENIARD, P., DULAC, A.M., ROCQUEFELTE, X., GRIGOROVA, V., LEBACQ, O., PASTUREL, A. & JOBIC, S. (2004): High potential positive materials for lithium-ion batteries: transition metal phosphates. *J. Phys. Chem. Solids* **65**, 229-233.

EVENTOFF, W., MARTIN, R. & PEACOR, D.R. (1972): The crystal structure of heterosite. *Am. Mineral.* **57**, 45-51.

FEHR, K.T., HOCHLEITNER, R., SCHMIDBAUER, E. & SCHNEIDER, J. (2007): Mineralogy, Mössbauer spectra and electrical conductivity of triphylite, $Li(Fe^{2+},Mn^{2+})PO_4$. *Phys. Chem. Minerals* **34**, 485-494.

FINGER, L.W. & RAPP, G., JR. (1969): Refinement of the structure of triphylite. *Carnegie Inst. Wash., Year book* **68**, 290-293.

FONTAN, F., HUVELIN, P., ORLIAC, M. & PERMINGEAT, F. (1976): La ferrisicklerite des pegmatites de Sidi-bou-Othmane (Jebilet, Maroc) et le groupe des minéraux à structure de triphylite. *Bull. Soc. fr. Minéral. Cristallogr.* **99**, 274-286.

FRANSOLET , A.-M., ABRAHAM, K. & SPEETJENS, J.-M. (1985): Evolution génétique et signification des associations de phosphates de la pegmatite d'Angarf-Sud, plaine de Tazenakht, Anti-Atlas, Maroc. *Bull. Minéral.* **108**, 551-574.

FRANSOLET, A.-M., ANTENUCCI, D., SPEETJENS, J.-M. & TARTE, P. (1984): An X-ray determinative method for the divalent cation ratio in the triphylite–lithiophilite series. *Mineral. Mag.* **48**, 373-381.

FRANSOLET, A.-M., KELLER, P. & FONTAN, F. (1986): The phosphate mineral associations of the Tsaobismund pegmatite, Namibia. *Contrib. Mineral. Petrol.* **92**, 502-517.

GELLER, S. & DURAND, J.L. (1960): Refinement of the structure of $LiMnPO_4$. *Acta Crystallogr.* **13**, 325-331.

HATERT, F. & BURKE, E. (2008): The IMA–CNMNC dominant-constituent rule revisited and extended. *Can. Mineral.* **46**, 717-728.

HATERT, F., OTTOLINI, L., FONTAN, F., KELLER, P., RODA-ROBLES, E. & FRANSOLET, A.-M. (2011b): The crystal chemistry of olivine-type phosphates. *Fifth Int. Symp. on Granitic Pegmatites, PEG2011, Assoc. Geol. Argentina, ser. D, Publ. Especial* **14**, 103-105 (abstr.).

HATERT, F., OTTOLINI, L. & SCHMID-BEURMANN, P. (2011a): Experimental investigation of the alluaudite + triphylite assemblage, and development of the Na-in-triphylite geothermometer: applications to natural pegmatite phosphates. *Contrib. Mineral. Petrol.* **161**, 531-546.

KANG BYOUNGWOO & CEDER, G. (2009): Battery materials for ultrafast charging and discharging. *Nature* **458**, 190-193.

KIM SUNG-WOOK, KIM JONGSOON, GWON HYEOKJO & KANG KYOUNGWOO (2009): Phase stability study of $Li_{1-x}MnPO_4$ ($0 < x < 1$) cathode for Li rechargeable battery. *J. Electrochem. Soc.* **156**, A635-A638.

LOSEY, A., RAKOVAN, J., HUGHES, J.M., FRANCIS, C.A. & DYAR, M.D. (2004): Structural variation in the lithiophilite–triphylite series and other olivine-group structures. *Can. Mineral.* **42**, 1105-1115.

MASON, B. (1941): Minerals of the Varuträsk pegmatite. XXIII. Some iron–manganese phosphate minerals and their alteration products, with special reference to material from Varuträsk. *Geol. Fören. Stockholm Förh.* **63**(2), 117-175.

MOORE, P.B. (1972): Natrophilite, $NaMnPO_4$, has ordered cations. *Am. Mineral.* **57**, 1333-1344.

OKADA, S., SAWA, S., EGASHIRA, M., YAMAKI, J., TABUCHI, M., KAGEYAMA, H., KONISHI, T. & YOSHINO, A. (2001): Cathode properties of phosphoolivine $LiMPO_4$ for lithium secondary batteries. *J. Power Sources* **97-98**, 430-432.

OTTOLINI, L., BOTTAZZI, P. & VANNUCCI, R. (1993): Quantification of lithium, beryllium and boron in silicates by secondary ion mass spectrometry using conventional energy filtering. *Anal. Chem.* **65**, 1960-1968.

OXFORD DIFFRACTION (2007): *CrysAlis CCD and CrysAlis RED*, *version 1.71*. Oxford Diffraction, Oxford, England.

PADHI, A.K., NANJUNDASWAMY, K.S. & GOODENOUGH, J.B. (1997): Phosphoolivines as positive materials for rechargeable lithium batteries. *J. Electrochem. Soc.* **144**, 1188-1194.

PALACHE, C., BERMAN, H. & FRONDEL, C. (1951): *The System of Mineralogy* (7th ed.). John Wiley and Sons, New York, N.Y.

PROSINI, P.P., LISI, M., ZANE, D. & PASQUALI, M. (2002): Determination of the chemical diffusion coefficient of lithium in $LiFePO_4$. *Solid State Ionics* **148**, 45-51.

QUENSEL, P. (1937): Minerals of the Varuträsk pegmatite. I. The lithium–manganese phosphates. *Geol. Fören. Stockholm Förh.* **59**, 77-96.

RAVET, N., ABOUIMRANE, A. & ARMAND, M. (2003): On the electronic conductivity of phospho-olivines as lithium storage electrodes. *Nat. Mater.* **2**, 702.

RENNER, B. & LEHMANN, G. (1986): Correlation of angular and bond length distortion in TO_4 units in crystals. *Z. Kristallogr.* **175**, 43-59.

RODA, E., FONTAN, F., PESQUERA, A. & VELASCO, F. (1996): The phosphate mineral association of the granitic pegmatites of the Fregeneda area (Salamanca, Spain). *Mineral. Mag.* **60**, 767-778.

RODA, E., PESQUERA, A., FONTAN, F. & KELLER, P. (2004): Phosphate mineral associations in Cañada pegmatite (Salamanca, Spain): paragenetic relationships, chemical compositions, and implications for pegmatite evolution. *Am. Mineral.* **89**, 110-125.

RODA-ROBLES, E., FONTAN, F., PESQUERA PÉREZ, A. & KELLER, P. (1998): The Fe–Mn phosphate associations from the Pinilla de Fermoselle pegmatite, Zamora, Spain: occurrence of kryzhanovskite and natrodufrénite. *Eur. J. Mineral.* **10**, 155-167.

RODA-ROBLES, E., VIERA, R., PESQUERA, A. & LIMA, A. (2010): Chemical variations and significance of phosphates from the Fregeneda–Almendra pegmatite field, Central Iberian Zone (Spain and Portugal). *Mineral. Petrol.* **100**, 24-34.

SCHALLER, T. (1912): New manganese phosphates from the gem tourmaline field of Southern California. *J. Wash. Acad. Sci.* **2**(6), 143-145.

SHANNON, R.D. (1976): Revised effective ionic radii and systematic studies of interatomic distances in halides and chalcogenides. *Acta Crystallogr.* **A32**, 751-767.

SHELDRICK, G.M. (2008): A short history of *SHELX*. *Acta Crystallogr.* **A64**, 112-122.

SONG YANNING, YANG SHOUFENG, ZAVALIJ, P.Y. & WHITTINGHAM, M.S. (2002): Temperature-dependent properties of $FePO_4$ cathode materials. *Mater. Res. Bull.* **37**, 1249-1257.

TAKAHASHI, M., TOBISHIMA, S., TAKEI, K. & SAKURAI, Y. (2002): Reaction behavior of $LiFePO_4$ as a cathode mate-

rial for rechargeable lithium batteries. *Solid State Ionics* **148**, 283-289.

WANG, X.J., ZOU, T.R., XU, J.G., YU, X.Y. & QIU, Y.Z. (1981): *Study of Pegmatite Minerals of the Altai Region*. Science Publishing House, Beijing, People's Republic of China (in Chinese).

WILSON, A.J.C. (1992): *International Tables for X-ray Crystallography*, Vol. C. Kluwer Academic Press, London, U.K.

YAKUBOVICH, O.V., SIMONOV, M.A. & BELOV, N.V. (1977): The crystal structure of a synthetic triphylite, LiFe[PO_4]. *Sov. Phys. Dokl.* **22**, 347-350.

YANG SHOUFENG, SONG YANNING, NGALA, K., ZAVALIJ, P.Y. & WHITTINGHAM, M.S. (2003): Performance of $LiFePO_4$ as lithium battery cathode and comparison with manganese and vanadium oxides. *J. Power Sources* **119-121**, 239-246.

ZHANG, A.C., WANG, R.C., HU, H., ZHANG, H., ZHU, J.C. & CHEN, X.M. (2004): Chemical evolution of Nb–Ta oxides and zircon from the Koktokay No. 3 granitic pegmatite, Altai, northwestern China. *Mineral. Mag.* **68**, 739-756.

ZHU, J.C., WU, C.N., LIU, C.S., LI, F.C., HUANG, X.L. & ZHOU, D.S. (2000): Magmatic-hydrothermal evolution and genesis of Koktokay No. 3 rare metal pegmatite dyke, Altai, China. *Geol. J. China Universities* **6**, 40-52 (in Chinese).

Received July 21, 2011, revised manuscript accepted July 1, 2012.